Quaternary Science Reviews 325 (2024) 108472

Contents lists available at ScienceDirect

Quaternary Science Reviews

journal homepage: www.elsevier.com/locate/quascirev

Millennial-scale changes in the environment, ice conditions, and deep-water ventilation at the Detroit–Tenji Seamounts, Northwest Pacific, over the last 43 kyr

Sergey A. Gorbarenko [a,*], Xuefa Shi [b], Aleksandr A. Bosin [a], Yanguang Liu [b], Yuriy P. Vasilenko [a], Elena A. Yanchenko [a], Aleksandr N. Derkachev [a], Ivan S. Kirichenko [c], Antonina V. Artemova [a], Tatyana A. Velivetskaya [d], Olga Yu Psheneva [a]

[a] V.I. Il'ichev Pacific Oceanological Institute, Far East Branch of the Russian Academy of Sciences, Vladivostok, Russia
[b] Key Laboratory of Marine Geology and Metallogeny, First Institute of Oceanography, Ministry of Natural Resources, Qingdao, China
[c] Geology and Mineralogy Institute, Siberian Branch of the Russian Academy of Sciences Novosibirsk, Russia
[d] Far Eastern Geological Institute, FEB of RAS, Vladivostok, Russia

ARTICLE INFO

Handling editor: Dr I Hendy

Keywords:
Detroit seamount
Planktic foraminifera
Benthic foraminifera
Icebergs
Sea-ice
Deep water ventilation

ABSTRACT

The Western Subarctic Gyre (WSG) in the North Pacific represents the termination of the Atlantic Meridional Overturning Circulation (AMOC). It has been strongly influenced by periodic glaciations of adjacent landmasses, orbital- and millennial-scale variability of its environment, and ventilation, which, to date, have been poorly studied. In this study, we investigated sediment core LV76-21 recovered from the Detroit Seamount using several productivity and lithological proxies, δ^{18}O records of planktic and benthic foraminifera (δ^{18}Opf and δ^{18}Obf), AMS ^{14}C data. We also used the published results from three well-dated cores from the Detroit and Tenji Seamounts. Comparison of the δ^{18}Opf and δ^{18}Obf records allowed us to establish iceberg discharge events 1 and 1' at 39–36.8 and 42–40 ka, respectively, in the WSG over the last 43 kyr. This was accompanied by considerable lightning of δ^{18}Opf relative to the coeval δ^{18}Obf values. The lithological results have also shown variable sea-ice influence on the regional environment during Marine Isotope Stage 3 and particularly 2, with sea ice extensions at 28.5–25.5 ka and 17.6–16.6 ka, and its significant loss since the Bølling–Allerød warming. We used high resolution δ^{18}Obf records from studied cores as a subtle proxy of contribution of North Atlantic Deep Water (NADW) to Lower Circumpolar Deep Water (LCDW), which originating from around Antarctica and have slightly different δ^{18}Obf values, in order to reconstruction of its spatial variability in the context of regional deep-water ventilation. The contribution of NADW to LCDW in the ventilation of the western flank of Detroit Seamount significantly increased during the interglacial and long-lasting Dansgaard–Oeschger interstadials, which was synchronous with the AMOC intensification. Over the last 43 kyr, the deep water of its eastern flank has been constantly ventilated by the LCDW with low contribution of NADW.

1. Introduction

Analyses of oxygen isotope records from Greenland ice cores have shown that the last glacial cycle was interrupted by millennial-scale climate oscillations with irregular periodicity (Dansgaard et al., 1982, 1993; Johnsen et al., 1992). Prominent and fast abrupt warmings (interstadials), followed by gradual cooling and cold events (stadials), known as Dansgaard–Oeschger (DO) oscillations, have been recorded in Greenland ice cores (Dansgaard et al., 1993; Grootes et al., 1993). Heinrich (1988) found irregular sequences of ice-rafted debris (IRD) events in the Northeast Atlantic over the last 130 kyr, forced by iceberg discharge that drained the Laurentide Ice Sheet into the North Atlantic. These are known as cold Heinrich events (HEs) (Alley and MacAyeal, 1994). Bond et al. (1993) also observed several abrupt temperature oscillations during the last glaciation in northern Atlantic surface water, which closely matched the DO events in Greenland. They confirmed that several ocean–atmosphere shifts, combined in cycles with a periodicity of 10–15 kyr, culminated in pronounced cooling forced by HEs. This

* Corresponding author.
E-mail address: gorbarenko@poi.dvo.ru (S.A. Gorbarenko).

https://doi.org/10.1016/j.quascirev.2023.108472
Received 7 December 2022; Received in revised form 24 August 2023; Accepted 13 December 2023
Available online 29 December 2023
0277-3791/

predates the longest and largest DO interstadials (DOIs). Subsequently, DO oscillations were observed in atmospheric oscillations as shifts in continental dust and atmospheric sea salt content (Mayewski et al., 1997). DO oscillations have also been recorded in several marine and lacustrine archives (Altabet et al., 2002; Jones et al., 2002; Kienast and McKay, 2001; Schulz et al., 1998). Sediments from the California margin have shown surface and intermediate water fluctuations forced by the abrupt reorganization of atmospheric circulation over the North Pacific, which have occurred synchronously with Greenland oscillations (Hendy and Kennett, 1999). DO-like oscillations have also been found in millennial-scale activity in East Asian and the Indo-Asian monsoon. They have been identified in oxygen isotope fluctuations within precisely dated cave stalagmites (Cheng et al., 2006; Gebregiorgis et al., 2016; Wang et al., 2001). The influence of millennial DO oscillations on the subarctic North Pacific climate, ice conditions, and regional deep-water ventilation is studied extremely weak. The millennial-scale paleoclimate and environmental history of the far NW Pacific have been constrained over the last 20 kyr (Keigwin, 1998; Keigwin et al., 1992; Max et al., 2012). The prolonged environmental history of the NW Pacific has been studied predominantly on orbital timescales (Galbraith et al., 2007; Gebhardt et al., 2008; Jaccard et al., 2005, 2010; Kiefer et al., 2001).

However, tracing the North Atlantic Deep Water (NADW)millennial-scale variability outside the Atlantic Ocean has attracted less attention. Using $\delta^{18}O$ data from diatoms, Maier et al. (2018) found evidence of freshwater injection from the North American Cordilleran Ice Sheet into the NE Pacific during HEs. Gorbarenko et al. (2022) found five periods of Western Subarctic Gyre (WSG) surface water freshening and a related decrease in planktic foraminiferal $\delta^{18}O$ ($\delta^{18}Opf$) because of iceberg meltwater derived from the Kamchatka glaciers over the last 190 kyr.

The relationship between glacial ice sheet formation on the northeastern Asian coast and related NW Pacific environmental changes is still under debate (Bigg et al., 2008; Brigham-Grette et al., 2003; Grosswald and Hughes, 2002; Lisitzin, 2002; McCarron et al., 2021). Investigations of the IRD in western North Pacific cores have suggested that during glacial periods this material could have been derived from calving icebergs from the Kamchatka and Koryak glaciers (Conolly and Ewing, 1970; Lisitzin, 2002; McCarron et al., 2021; McKelvey et al., 1995) and from sea ice from the northeastern Asian coast and western Alaska Province (Bigg et al., 2008; Lisitzin, 2002; VanLaningham et al., 2009).

In this study, we focused on the reconstruction of millennial-scale changes in climate, productivity, ice conditions, and deep-water ventilation of the WSG over the last 43 kyr. This was based on multi-proxy records from core LV76-21 recovered from the Detroit Seamount. We combined high-resolution $\delta^{18}O$ records of benthic foraminifera ($\delta^{18}Obf$)

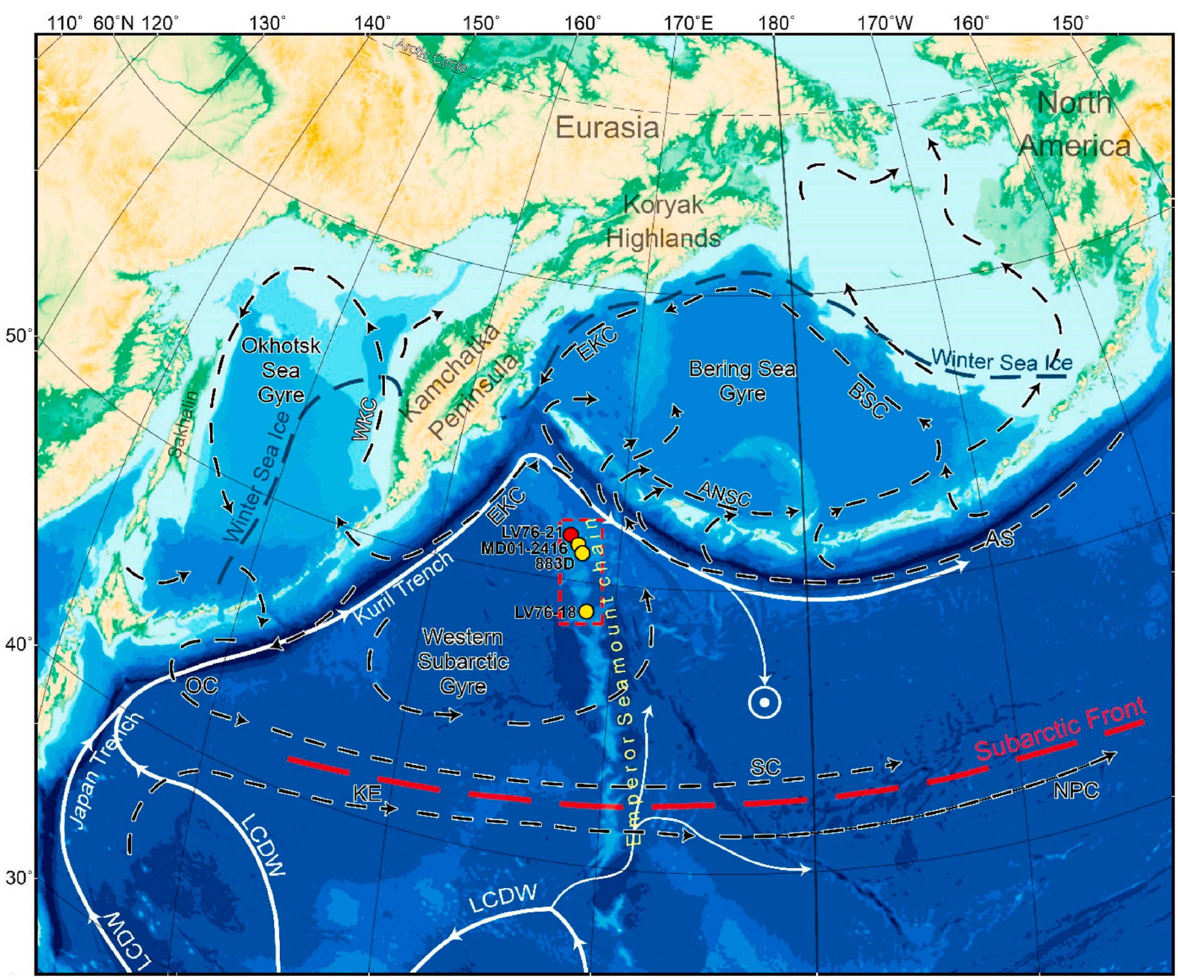

Fig. 1. Bathymetry, surface, and deep water currents of the northwest Pacific, Okhotsk, and the Bering seas, and the position of the core studied (LV76-21, red circle) and other cores used (MD01-2416, 883D, and LV76-18, yellow circles). Major surface water currents are shown by black dash arrows, labeled as follows: AS: Alaskan Stream; ANSC: Aleutian North Slope Current; BSC: Bering Slope Current; EKC: East Kamchatka Current; WKC: West Kamchatka Current; OC: Oyashio Current; SC: Subarctic Current; KE: Kuroshio Extension; and NPC: North Pacific Current. Schematic circulation of deep water masses are shown by white arrows according to Kawabe and Fujio (2010) and Owens and Warren (2001); LCDW: Lower Circumpolar Deep Water; circle with a center point shows upwelling of LCDW and its transformation into North Pacific Deep Water (NPDW). The area delimited by the red dashed line is shown in Fig. 7.

and δ^{18}Opf, several productivity proxies, benthic foraminiferal abundance (BFA), IRD records from core LV76-21and other published evidences from the Detroit–Tenji Seamount cores to reconstruct the regional influence of sea ice and icebergs over the last 43 ka. Comparison of high resolution δ^{18}Obf records, as subtle proxy of the different deep-water masses, from cores recovered from the western and eastern flanks of the Detroit–Tenji Seamounts allowed us to examine regional deep-water ventilation over the last 43 kyr.

2. Oceanographical setting

The subarctic North Pacific has four large-scale surface-water cyclonic circulation systems, namely the Alaskan Gyre in the NE Pacific, the WSG in the NW Pacific, the Bering Sea Gyre, and the Okhotsk Sea Gyre in the marginal seas (Emile-Geay et al., 2003; Favorite et al., 1976) (Fig. 1). The surface water hydrology of the WSG is outlined by the Alaskan Stream to the north, the East Kamchatka and Oyashio Currents to the west, and the Subarctic Current to the south (Fig. 1). North Pacific Intermediate Water (NPIW) is primarily formed in the Okhotsk Sea by winter sea ice formation and brine rejection (Talley, 1993). Modern deep-water formation in the North Pacific is hampered by low surface water salinity (Emile-Geay et al., 2003; Warren, 1983).

According to Talley (1993, 2011), global deep- and bottom-water overturning can be divided into two major interconnected global cells. One was the North Atlantic Deep Water (NADW) cell, a cell with dense water formation around the North Atlantic. The other was the Antarctic Bottom Water (AABW) cell, with dense water formation around Antarctica. They showed that when the NADW leaves the southern Atlantic, part of it enters into the Antarctic Circumpolar Current (ACC), upwells, and becomes the source for deep and bottom water formation around Antarctica.

The Lower Circumpolar Deep Water (LCDW), which comprises the remnant of NADW and mostly AABW, is transported from the ACC northward to the North Pacific, ventilate the Pacific and upwells with transformation into the North Pacific Deep Waters (NPDW) (Fuhr et al., 2021; Johnson, 2008; Kawabe and Fujio, 2010) (Fig. 1). The western branch of the LCDW flows northward along the Japan and Kuril Trenches, turns eastward at the northern end of the Emperor Seamount Chain, and fills the northeastern Pacific through the Aleutian Trench (Fig. 1, white lines). Some parts of the LCDW flowed northward along the eastern flanks of the Emperors (Fig. 1). Therefore, examining the sediment cores recovered at the Detroit and Tenji Seamounts, that is, the northern tip of the Emperors (Fig. 1), offers the unique potential to monitor past variability of deep-water circulation in the far northwestern Pacific.

3. Material and methods

Sediment core LV76-21 was recovered from the northwest of the Detroit Seamount (51°34.0′N, 167°15.7′E; water depth = 2769 m) (Fig. 1) using a gravity corer on the R/V "Akademik M.A. Lavrentyev" during the joint Russian–Chinese expeditions in 2016. The core sediments were predominantly grey–olive–grey terrigenous silty clay-clayey silt, with rare amounts of sand. The sediment was coarser at the 144–167 and 434–456 cm intervals. The upper 17 cm of the sediment was represented by an oxidized brown–grey–brown ooze. In the 0–38, 76–167, 356–364, 407–434, 456–475, and 519–546 cm intervals, the sediments were represented by weakly diatomaceous greyish–olive–olive ooze. The sediments at intervals of 0–144 cm and 519–546 cm were enriched with foraminiferal shells and were weakly enriched with foraminifera at intervals of 407–434 cm, 456–482 cm, and 546–557 cm. The lithological description showed three visible ash layers at depths of 364–366, 397–404, and 467–468.5 cm, with thin ash lenses at depths of 477–479 cm.

3.1. AMS ^{14}C dating

Eight monospecific samples of the planktic foraminifera *Neogloboquadrina pachyderma* (s) weighing 4–6 mg were selected from the >150-μm size fraction and measured at the Beta Analytic Radiocarbon Dating Laboratory (Table 1). Conventional accelerator mass spectrometry (AMS) ^{14}C ages were corrected to the reservoir age of the far NW Pacific according to Butzin et al. (2017) and Sarnthein et al. (2007) and calibrated to calendar ages using *Calib 8.20* with the IntCal20 calibration curve (Reimer et al., 2020). The reservoir age was taken as the average of the ages, according to Sarnthein et al. (2007) and Butzin et al. (2017).

3.2. Planktic and benthic foraminifera δ^{18}O analysis

Sediments for δ^{18}Opf and δ^{18}Obf analysis were sampled from core LV76-21 as 1 cm-thick slices in steps of 2–5 cm along the core length. The planktic foraminifera *N. pachyderma* (s.) were collected from the 150–250 μm sediment fraction and benthic *Uvigerina auberiana* and *Cibicidoides* spp. from the 250–350 μm fraction in each sample. The δ^{18}Opf and δ^{18}Obf values were measured at Tongji University (China) and the Far Eastern Geological Institute (Russia). Isotope measurements were performed at Tongji University using a Finnigan MAT 252 mass spectrometer. The results were validated against the Chinese National Carbonate Standard (GBW04405) and NBS-19. The standard deviation was 0.07‰ for δ^{18}O. Isotope measurements from the Far Eastern Geological Institute were analyzed using a Finnigan MAT 253 mass spectrometer with the modification of Velivetskaya et al. (2009) without preliminary roasting. The standard deviation of δ^{18}O values was ±0.05‰. All values are reported on the Pee Dee Belemnite (PDB) scale.

3.3. IRD analysis

Sediment for IRD assessment was sampled from 1 cm-thick slices in steps of 2–4 cm through the core. Samples with a dry weight of approximately 10 g were wet-sieved using a 150-μm sieve, decarbonized using 10% HCl, washed using distilled water, and dried. The ratio of the weight percentage of the decarbonized coarse fraction (CF; 150–2000 μm) relative to the weight of the dried bulk sediment (wt CF) was used as the IRD indicator, transferred into sediments by sea ice or icebergs. This is consistent with the commonly used size fraction of >150 μm for delimiting the IRD (Hemming, 2004). Data from the intervals of the visible tephra layers were excluded from the IRD record because this material was delivered to the sediment through the atmosphere rather than through ice; therefore, it was not an IRD. Given that the nearby Kamchatka Peninsula is an area of active volcanism, the IRD values may include terrigenous and volcanic particles. These particles experienced an earlier fallout during explosive volcanic eruptionswere captured by sea ice and icebergs, delivered to core location by sea ice and icebergs and released during its melting.

3.4. Productivity proxies

We used the calcium carbonate, total organic carbon (TOC), and chlorin content of the sediments as indicators of primary productivity in surface water. Total carbon and inorganic carbon contents were measured in 1 cm-thick sediment slices at 2 cm resolution using an AN-7529 coulometer (Gorbarenko et al., 1998). The TOC content of the sediment was calculated as the difference between the total and inorganic carbon contents. The sediment for chlorin determination was sampled in 1 cm-thick slices at a resolution of 1 cm. Chlorin content is the product of chlorophyll-*a* transformation in sediments and is a highly sensitive indicator of primary production. Chlorin content was measured using a Shimadzu UV-1650PC spectrophotometer according to an established method (Harris et al., 1996) with modifications (Zakharkov et al., 2007). Color b* values have been widely used as paleoproductivity proxy for the NW Pacific and its marginal seas

Table 1
AMS^{14}C dates of samples from core LV76-21.

Depth, cm	Material	Uncorrected AMS^{14}C age, yr	MRA1, yr	MRA2, yr	Mean MRA, yr	Corrected AMS^{14}C age, yr	Calibrated age, cal. yr
22	*N. pachyderma* (s.)	4670 ± 30	900	600	750 ± 150	3920 ± 180	4400
36	*N. pachyderma* (s.)	7410 ± 30	900	730	815 ± 85	6595 ± 115	7500
48	*N. pachyderma* (s.)	9800 ± 30	900	530	715 ± 185	9085 ± 215	10 200
130	*N. pachyderma* (s.)	13 010 ± 40	900	770	835 ± 65	12 175 ± 105	14 100
140	*N. pachyderma* (s.)	13 310 ± 40	900	700	800 ± 100	12 510 ± 140	14 700
160	*N. pachyderma* (s.)	13 680 ± 40	900	690	795 ± 105	12 885 ± 145	15 400
170	*N. pachyderma* (s.)	14 320 ± 40	450	580	515 ± 65	13 805 ± 105	16 700
188	*N. pachyderma* (s.)	15 580 ± 40	300	750	525 ± 225	15 055 ± 265	18 400

Note: MRA1 is the marine reservoir age according to Sarnthein et al. (2007); MRA2 is the marine reservoir age according to Butzin et al. (2017). All ages here and further are presented in yrs before 1950 AD.

(Nürnberg and Tiedemann, 2004; Riethdorf et al., 2013). Therefore, the color b* index, an indicator of diatom production and biogenic silica content in sediments, was measured at a 1 cm resolution onboard after sediment core splitting using a Konica Minolta CM-700 d spectrophotometer.

3.5. Magnetic susceptibility

The sediment magnetic susceptibility (MS) was measured onboard using a *Satis Geo KM-7* kappameter at a resolution of 1 cm. The sediment core was split, and half of the core was used for MS measurements. The sediment MS values indicate input of the terrigenous ferromagnetic and volcanogenic material into sediments.

3.6. Chemical element content

Briefly, 30 mg of sediment was sampled in 1 cm steps through the full core depth for elemental content analysis. The sediment was compressed into 5 mm-diameter tablets with a surface density = 0.13 g × cm^{-2}, following the methods of Phedorin et al. (2007). Elemental concentrations were measured with X-ray fluorescence using synchrotron radiation at the collective station VEPP 3 (Institute of Nuclear Physics, Novosibirsk, Russia), following the method of Piminov et al. (2016). We used the concentrations of Rb and Ti in the sediment as indicators of terrigenous material accumulation and the V content as a proxy for the redox condition at the bottom (Bodin et al., 2007; Colman et al., 1995; Goldberg et al., 2007). The Y/Rb ratio has been used as an indicator of volcanic material input (Gorbarenko et al., 2014).

3.7. Benthic foraminiferal

The variability in BFA in response to changes in primary productivity at the sea surface is considered a reliable indicator of paleoceanography (Gupta et al., 2006; Jorissen et al., 2007; Mackensen et al., 2000; Ohkushi et al., 2000). We studied the BF in core LV76-21 sediments sampled from 1 cm-thick slices. All the samples were dried, weighed, and wet-sieved using a 63-μm sieve. The benthic foraminifera shells were picked and counted from the 63–250 μm sediment fraction. In total, 222 samples were analyzed at an average resolution of 2.5 cm (range: 1–5 cm). Almost all the samples had sufficient microfossils for representative evaluation, except for the 365, 398–408, 435–440, 444–465, and 490–510 cm intervals, where foraminifera were rare or absent. We focused on the total BFA, expressed as the number of shells per 1 g of dry sediment (# specimens × g^{-1}).

4. Results and discussion

4.1. Age model

The age model construction of the core studied was based on AMS ^{14}C data, records of δ^{18}O of *Uv. auberiana* ($\delta^{18}O_{Ua}$), *Cibicidoides* spp., correlation of abrupt increases in the productivity and some lithological proxies with related DOIs, and tephrochronology (Fig. 2).

Ash layers at depths of 364–366 and 397–404 cm, which are strongly outlined with peaks of wt% CF, have not been previously identified. Based on the chemical composition of the ash layer at 467–468.5 cm (Fig. S1), we identified it as a chemical analog of the ash found earlier in the sediment of ODP Site 883D (Bigg et al., 2008) and in other NW Pacific cores (Derkachev et al., 2023) at an age of approximately 40 ka (Fig. S2). Age of 467–468.5 cm tephra was used to control for the age model construction. The sedimentation rates were calculated and intervals of visible ash layers were excluded. The deposition time for these ash layers was assumed to be 10 years.

A compilation of 63 independently dated speleothem records (Corrick et al., 2020) showed that abrupt warming in Greenland-like DO cycles (DO Interstadial) occurred synchronously with millennial-scale climate changes of monsoon records. Therefore, the Greenland ice core and monsoon chronology can provide a coherent framework for abrupt climate changes in the Northern Hemisphere. This is consistent with global atmospheric teleconnections related to DO cycles in Greenland (Markle et al., 2017). It was shown that in the north Pacific and its marginal seas (Bering sea, Okhotsk Sea and Japan Sea), an abrupt climate warming related with DOI led to increases in the productivity due to more favorable environmental conditions for primary production – surface water warming, less influence of sea ice and more prolonged and active vegetation season (Gorbarenko et al., 2010; Hendy et al., 2002; Riethdorf et al., 2013; Schlung et al., 2013; Seki et al., 2002). Coeval, an abrupt climate warming led to decrease relative content of terrigenous materials in sediments, indicated by Ti and Rb (Goldberg et al., 2007) In this study, we used records of calcium carbonate, chlorin, TOC, BFA, and the color b* index as proxies for primary productivity and Rb and Ti content as typical terrigenous proxies in the North Pacific (Fig. 2). Such a correlation of the productivity and lithological proxies, together with available AMS datum and age of the tephra layer at 467–468.5 cm (nearly 40 ka), allowed us to determine the positions of DOIs 11, 10, 9, 8, 7, 6, 5, 4, 1 and 0 (Fig. 2). The established depth of onset of the long-lasting DOI 8 (432 cm) is well characterized by an increase in productivity proxies and a coeval decrease in terrigenous proxies in sediments. The positions of DOI 0 and 1 were consistent with that identified from the AMS ^{14}C data and changes in productivity and lithological proxies determined the onset of Holocene and Bølling–Allerød warming, respectively. Less pronounces DOI 4 was marked only by increase in $CaCO_3$ content; while was followed by heaviest δ^{18}O of *Uv. auberiana,* consistently with onset of cold MIS 2.

In the results, the AMS ^{14}C data, correlation of productivity and lithological proxies with DOI, δ^{18}O record of benthic foraminifera *Uv. Auberiana* and age of 467–468.5 cm tephra were used for determine ages of key time points of studied core (Table 2). Linear interpolation was used to calculate the ages between key time points and the age-depth model was calculated for the studied sediment core using Bayesian modelling with software Bacon 2.2 (Blaauw and Christen, 2011) (Fig. 3).

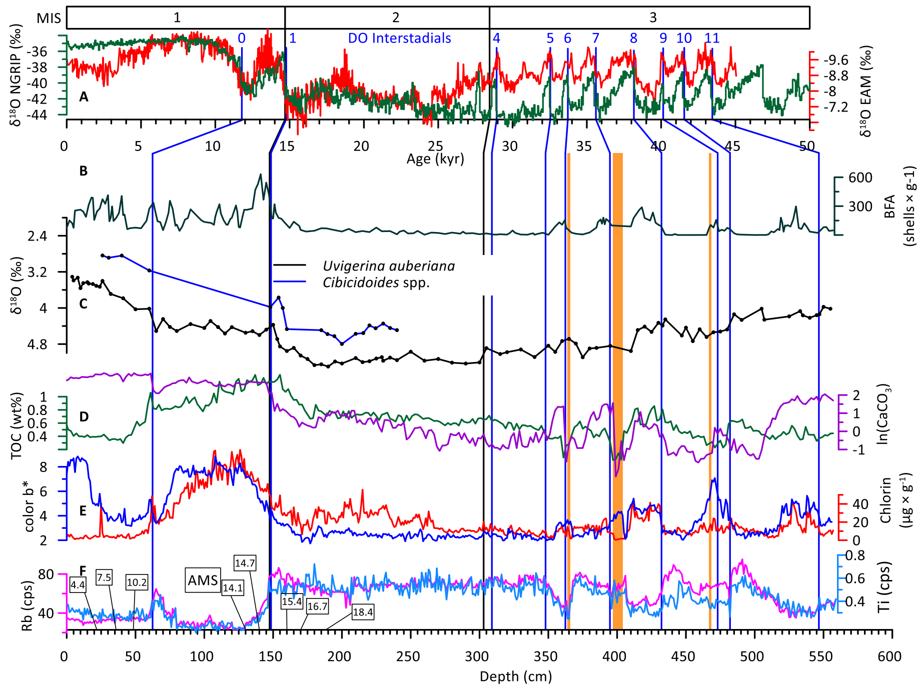

Fig. 2. Age model of core LV76-21. We used AMS ^{14}C data, records of δ^{18}Obf, and correlations of abrupt increases in productivity and some lithological proxies with the Dansgaard–Oeschger interstadials (DOIs) 11–0. A, Chronology of DOIs 11–0 according to the δ^{18}O record of the North Greenland Ice Core Project (NGRIP) on the GICC05 timescale (Rasmussen et al., 2014). B, Records of benthic foraminifera abundance (BFA). C, Records of δ^{18}Obf for *Uv. auberiana* and *Cibicidoides* spp. D, Records of total organic carbon (TOC) and calcium carbonate ($CaCO_3$) contents. E, Records of color b* and chlorin content. F, Record of Rb and Ti content. Calendar AMS ^{14}C data are also shown at the bottom. Orange bars show tephra layers.

Table 2
Key time points of core LV76-21 sediments based on AMS^{14}C data, correlation of abrupt increases in productivity and lithological proxies with DOIs, and tephrochronology.

Depth, cm	Methods	Age, cal yr	Sedimentation rate, cm/kyr
22	AMS age	4400	5.00
36	AMS age	7500	4.52
48	AMS age	10 200	4.44
62.5	DOI 0	11 650	10.00
130	AMS age	14 100	27.55
140	AMS age	14 700	16.67
160	AMS age	15 400	28.57
170	AMS age	16 700	7.69
188	AMS age	18 400	10.59
307	DOI 4	28 850	11.39
348	DOI 5	32 450	11.39
363	DOI 6	33 690	12.10
395	DOI 7	35 430	18.39
432	DOI 8	38 170	13.50
473	DOI 9	40 110	21.13
483	DOI 10	41 410	7.69
547	DOI 11	43 290	34.04

Note: AMS – accelerator mass spectrometry.

4.2. Millennial-scale icebergs and sea-ice influences on regional environmental change

Records of the IRD and terrigenous and volcanic material proxies, that is, MS, and the Y/Rb ratio, have shown that the environmental conditions of the Detroit Seamount region were strongly influenced by material from adjacent land through ice formation and water currents in the past, especially during periods of glaciation and deglaciation (Fig. 4). This is consistent with evidence from the far NW Pacific (Bigg et al., 2008; Conolly and Ewing, 1970; Keigwin et al., 1992; Lisitzin, 2002). Volcanic activity in the surrounding land (Bindeman et al., 2010; Ponomareva et al., 2021) has strongly influenced continental and marine sedimentation.

Considering the proximity of the study area to land and following the evidence of Hemming (2004) for the North Atlantic and Gorbarenko et al. (2022) for the NW Pacific, the δ^{18}O of *N. pachyderma* (s.) ($\delta^{18}O_{Np}$) records obtained allowed us to separate the debris rafted by icebergs from that rafted by sea ice. Therefore, it is likely that episodic lightning of $\delta^{18}O_{Np}$ relative to coeval δ^{18}Obf, which significantly exceeded the potential temperature effect, was driven by iceberg discharge. This was followed by decreases in surface water salinity in the WSG since a δ^{18}O values of continental ice sheets at moderate and high latitudes are relatively low (−20–30 ‰) (NGRIP members, 2004). This is in contrast to sea ice which has not undergone significant oxygen isotopic fractionation. Therefore, melting icebergs calved from the nearby Kamchatka–Koryak glaciers have likely significantly decreased the δ^{18}O of the WSG surface water and therefore δ^{18}Opf. A comparison of the LV76-21 core $\delta^{18}O_{Np}$ records with the benthic δ^{18}O stack LR04 shows two iceberg discharge events (IDEs), 1 and 1′, at 39–36.8 and 42–40 ka, respectively (Fig. 4E). IDE 1 started after the DO stadial 9 coeval with a large IRD peak and continued through DO Cycle. IDE 1’ started from DO stadial 11 and continued during DOIs 10–9 and was more weakly expressed by $\delta^{18}O_{Np}$.

To clarify the existence and timing of the IDEs in the WSG, we compared the IDEs established in core LV76-21 with those reconstructed using a similar approach in dated cores from the Detroit Seamount, namely MD01-2416 (Gebhardt et al., 2008), ODP Site 883D (Kiefer et al., 2001), and Tenji Seamount core LV76-18 (Gorbarenko et al., 2022) (Fig. 5).

An age model of the MD01-2416 core sediments was established according to the original AMS ^{14}C and magnetic paleointensity data of Gebhardt et al. (2008). Following the same approach, the age model for Site 883D was established based on the data of Kiefer et al. (2001) with modifications (Fig. S2, Table S1). The age model for core LV76-18 sediments was established according to Gorbarenko et al. (2022). For each core, we presented records of $\delta^{18}O_{Np}$ and $\delta^{18}O_{Ua}$, and the IRD data and productivity proxies were coupled over the last 43 kyr. Records of

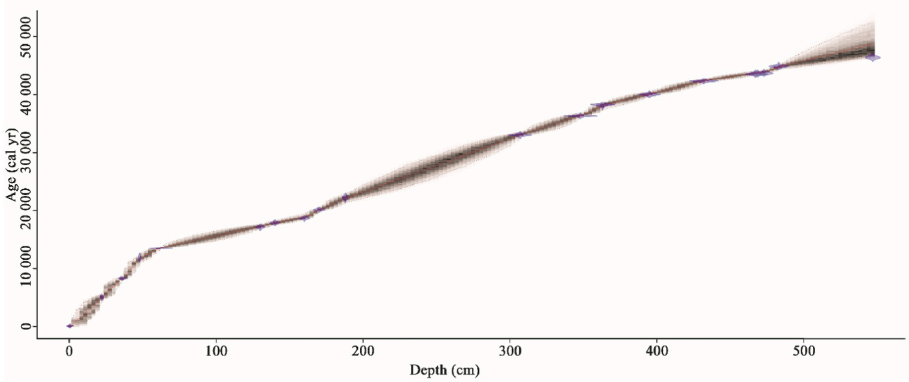

Fig. 3. Age model of sediment core LV76-21 calculated using Bayesian approach.

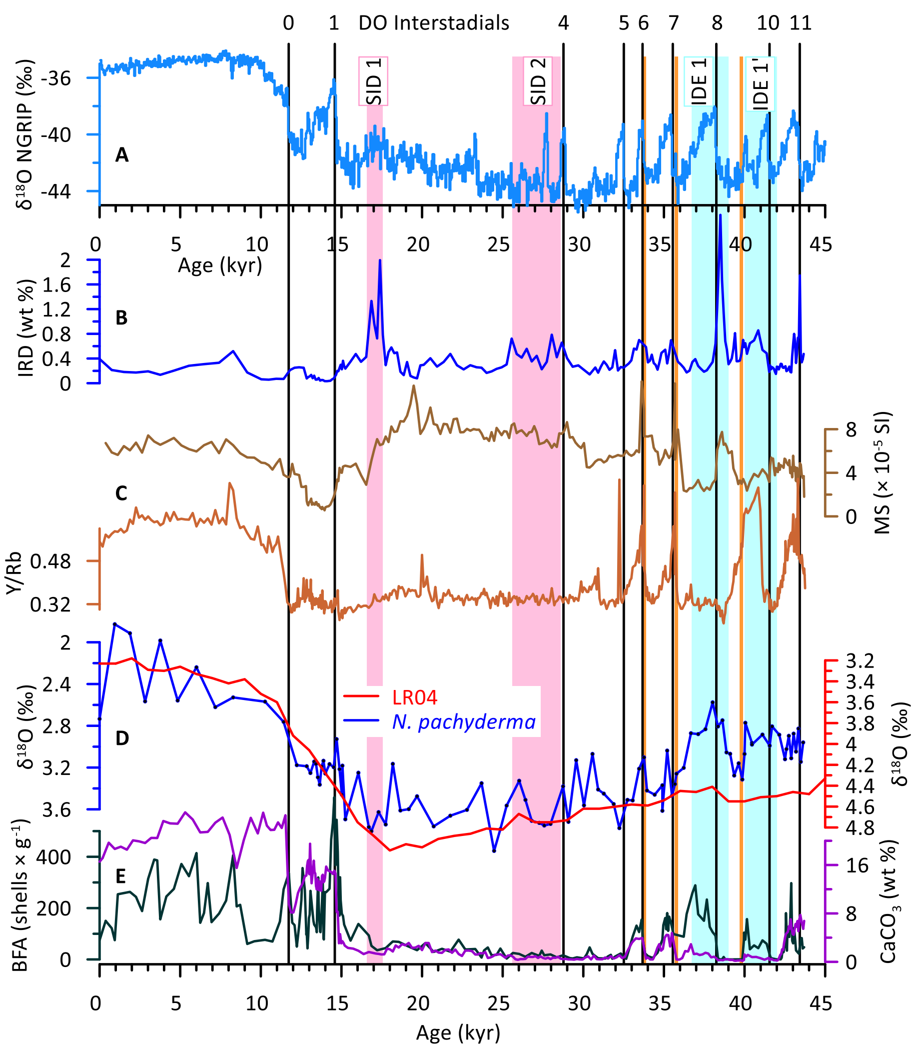

Fig. 4. Sea-ice and iceberg rafted debris (IRD) accumulation in core LV76-21 over the last 43 kyr. A, Dansgaard–Oeschger (DO) interstadials according to the $\delta^{18}O$ record of the North Greenland Ice Core Project (NGRIP) on the GICC05 timescale (Rasmussen et al., 2014). B, IRD (weight % of decarbonated sediment fraction 150–2000 μm). C, Volcanic material input indicated by magnetic susceptibility (MS) and Y/Rb ratio. D, Comparison of records of $\delta^{18}O$bf stack LR04 (Lisiecki and Raymo, 2005) and $\delta^{18}O_{Np}$ of core LV76-21. E, Productivity responsible proxies, that is, benthic foraminiferal abundance (BFA) and $CaCO_3$ content. Increased sea-ice debris (SID) events are shown by pink bars over MIS 2. Iceberg discharge events (IDEs) 1 and 1′ (blue bars) are indicated by significant lightning of $\delta^{18}O$Np relative to coeval $\delta^{18}O$bf values.

$\delta^{18}O_{Np}$ and $\delta^{18}O_{Ua}$ in other WSG cores also demonstrated episodic IDEs during MIS 3, which are similar to those in core LV76-21 (Fig. 4E, G, and I). The lightning of $\delta^{18}O_{Np}$ relative to the coeval $\delta^{18}O_{Ua}$ or $\delta^{18}O_{bf}$ stack LR04 during IDE 1 was equal to 0.55, 0.6, 0.4, and 0.6‰ for cores LV76-21, 883D, LV76-18, and MD01-2416, respectively (Fig. 5C, E, G, I). These $\delta^{18}O_{Np}$ deviations considerably exceeded the potential temperature effect at the depths of the regional pycnocline (60–100 m), which is the habitat of this species (Riethdorf et al., 2013). This is

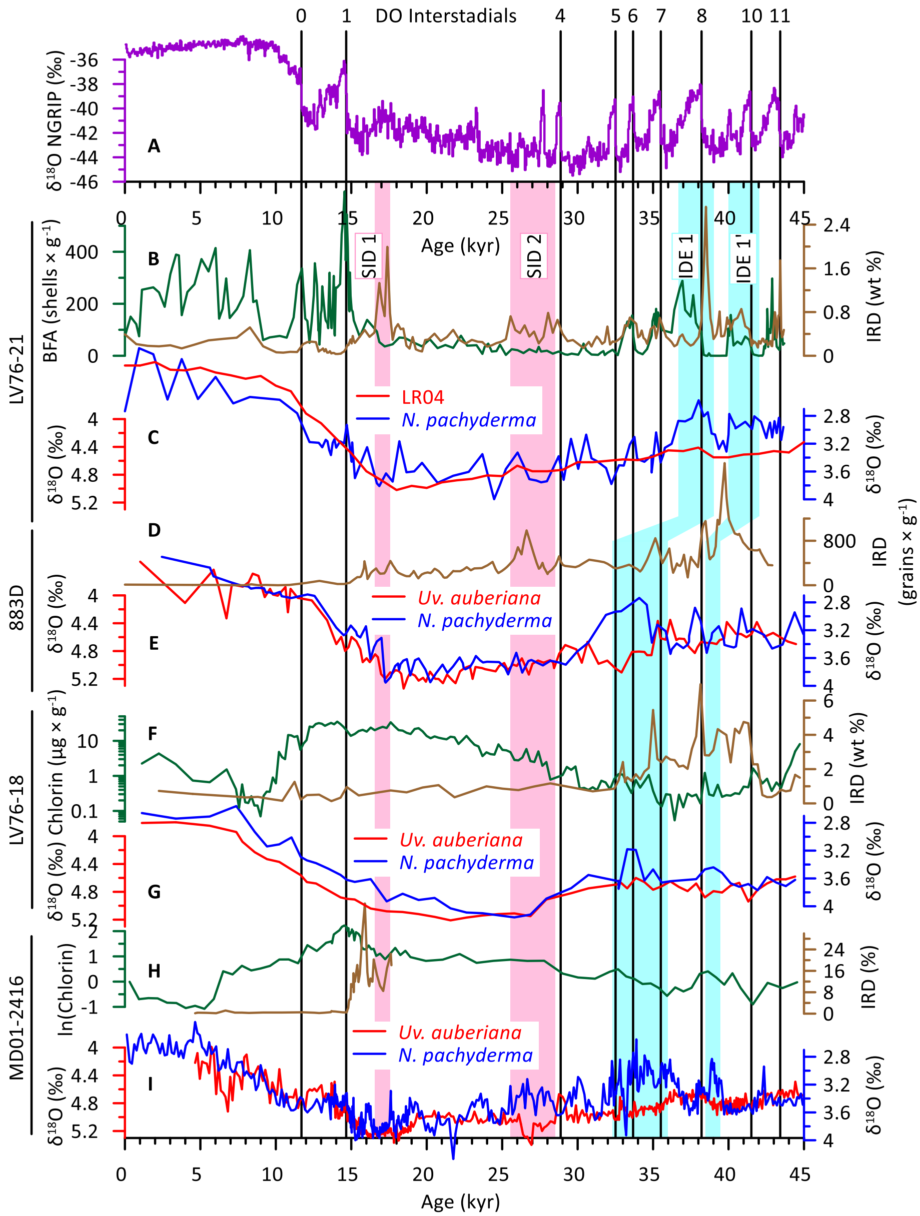

Fig. 5. Compiled iceberg discharge events (IDEs) and sea-ice debris (SID) events at the Detroit–Tenji Seamounts based on coupled records of δ^{18}O planktic and benthic foraminifera (δ^{18}Opf and δ^{18}Obf, respectively), ice-rafted debris (IRD) values, and productivity proxies recorded in cores LV76-21, MD01-2416, 883D, and LV76-18 over the last 43 kyr. A, Dansgaard–Oeschger (DO) interstadials according to the δ^{18}O record of the North Greenland Ice Core Project (NGRIP) on the GICC05 timescale (Rasmussen et al., 2014). B, records of benthic foraminiferal abundance (BFA) and IRD in core LV76-21. C, Comparison of δ^{18}Obf records for stack LR04 and $\delta^{18}O_{Np}$ for core LV76-21. D, IRD record for core 883D. E, G, and I, Comparison of records of $\delta^{18}O_{Np}$ and $\delta^{18}O_{Ua}$ for cores 883D, LV76-18, and MD01-2416, respectively. F and H, IRD and chlorin contents in cores LV76-18 and MD01-2416, respectively. Some differences in the ages of IDEs between the cores are likely due to inaccuracies in the age models and strong volcanic material inputs via regional sedimentation. IDEs and SID events are shown as for Fig. 4.

because one degree of water warming leads to a decrease in carbonate δ^{18}O at approximately 0.25‰ (Duplessy et al., 2002; Shackleton, 1974). Meanwhile, temperature changes at depths of 60–100 are usually several times less than at the surface. Therefore, if we convert the observed $\delta^{18}O_{Np}$ deviations into the water temperature alone, the resulting changes significantly exceed the glacial–interglacial global surface water temperature changes at moderate latitudes (3–4 °C) (Shakun et al., 2012). Therefore, it is likely that the observed $\delta^{18}O_{Np}$ changes were driven by a decrease in water δ^{18}O from iceberg melting. There was a slight discrepancy in the IDE ages between core LV76-21 and cores 883D, LV76-18, and MD01-2416 (Fig. 5). This was likely caused by inaccuracies in the age model construction and down-core variability of the sedimentation rates in these cores. Sedimentation in the WSG was significantly influenced by the strong episodic input of eruptive material from the volcanically active Kamchatka–Kurile area (Bindeman et al., 2010; Braitseva et al., 1995, 2005; Ponomareva et al., 2021).

The IRD record and related accumulation of terrigenous (MS) and volcanic (Y/Rb and MS) materials (Fig. 4) has shown that the WSG environment was also significantly affected by sea ice during the glacial and deglaciation periods. These events were not accompanied by significant lightning of $\delta^{18}O_{Np}$ relative to coeval δ^{18}Obf. The IRD and related records from several WSG cores (Fig. 5B, D, F, H) concordantly showed elevated values with episodic fluctuations during MIS 3 and 2, and a drop to approximately zero following the onset of B/A warming. During MIS 2, the IRD records of WSG cores show two periods of significant growth in the IRD transported by sea ice (sea-ice debris events, SIDs 1 and 2) over 17.6–16.6 and 28.5–25.5 ka, respectively (Figs. 3 and

4). These events were likely induced by the intensification of sea ice formation in the Bering Sea and far NW Pacific. The formation of SID 2 was likely triggered by a substantial global sea-level drop at approximately 30 ka (Lambeck et al., 2014; Yokoyama et al., 2018). Sea - level drop was likely accompanied by a large southward shift of the coastline in the Bering Sea and enhanced sea ice formation by strong northerly winds. The increase in sea ice formation in the Bering Sea since the onset of MIS 2 also led to the intensification of NPIW formation because of brine rejection into the underlying water (Knudson and Ravelo, 2015; Worne et al., 2019). SID 1 occurred nearly during HE 1, the coldest period of the Last Glacial Maximum (LGM), under severe environmental conditions.

After the IRD drop at the onset of B/A warming, which indicate on decrease in ice influence in the WSG, there was an IRD rise during the YD cold event. This was driven by the renewal of regional sea ice formation related to climate cooling (Fig. 5). An increase in the IRD and Y/Rb index, which are responsible for volcanic material input during the Holocene in core LV76-21 (Fig. 5B), was likely induced by the intensification of the Kamchatka volcanic activity (Bindeman et al., 2010; Ponomareva et al., 2017) with coeval ash input via atmosphere/surface water currents.

4.3. NADW contribution to the WSG deep-water ventilation; orbital- and millennial-scale changes

The Atlantic Meridional Overturning Circulation (AMOC) plays an

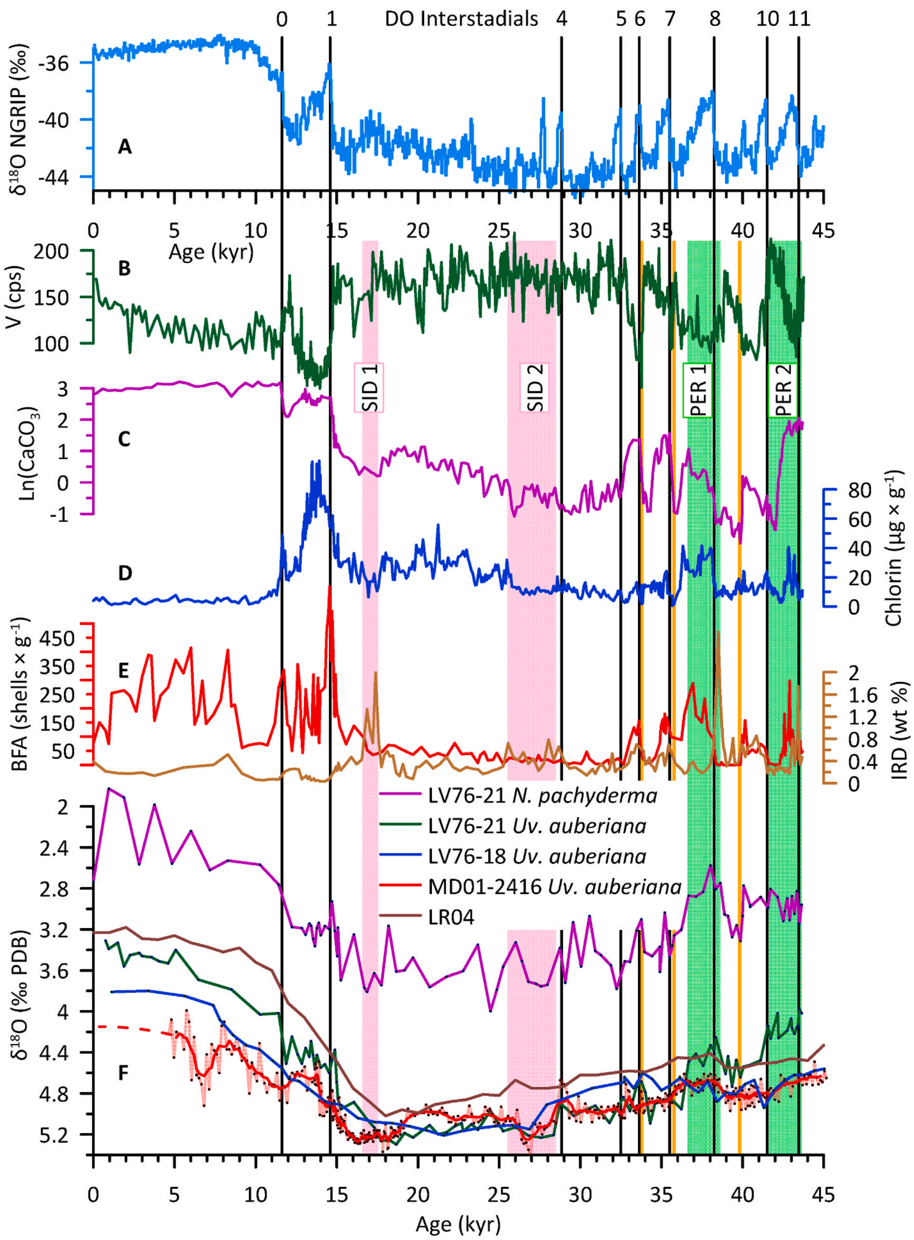

Fig. 6. Deep water ventilation and productivity changes over the last 43 kyr recorded in cores LV76-21, LV76-18, and MD01-2416. A, Dansgaard–Oeschger (DO) interstadials according to the δ^{18}O record from the North Greenland Ice Core Project (NGRIP) on the GICC05 timescale (Rasmussen et al., 2014). B, Record of vanadium content. C, Record of calcium carbonate content. D, Record of chlorin content. E, Records of ice-rafted debris (IRD) and benthic foraminiferal abundance (BFA). F, Records of $\delta^{18}O_{Np}$ and $\delta^{18}O_{Ua}$ from core LV76-21, benthic stack LR04 (Lisiecki and Raymo, 2005), and $\delta^{18}O_{Ua}$ from cores MD01-2416 and LV76-18 (Gebhardt et al., 2008; Gorbarenko et al., 2022). Sea-ice debris events (SIDs) and the Younger Dryas (YD) are shown by pink and yellow bars, respectively, according to Figs. 3 and 4. Green bars show periods of increase in contribution of NADW to LCDW in the ventilation of the western flank of Detroit Seamount during the glacial period.

important role in the formation of the global conveyor belt and global climate change (Broecker, 1991; Rahmstorf, 2002; Talley, 2011). The intensity of the AMOC decreased substantially, shoaled during HE 1, resumed at the onset of the B/A warming event, and was active during the subsequent interglacial (McManus et al., 2004). Based on two independent chemical water tracers measured in the sediment core from subtropical northwest Atlantic, Böhm et al. (2015) documented that over the last glacial cycle, the AMOC also declined considerably during most of the DO stadials. This was particularly the case during HEs, and it was activated during DOIs and particularly during long-lasting DOIs, which, likely, may to be traced in the North Pacific deep water circulation as well.

Today, and likely during the Late Pleistocene, the deep waters of the North Pacific were ventilated by southern-sourced AABW/LCDW, originating around the Antarctic, and by NADW, originating in the North Atlantic and via the Southern Ocean, before being transferred into the Pacific (Matsumoto, 2007; Stuiver et al., 1983; Talley, 2011; Talley, 2013; Kawabe and Fujio, 2010; Fuhr et al., 2021). The global ocean map of the NADW fraction in the modern balance of deep water below 1500 m by Matsumoto (2007) estimated that the fraction of NADW in the far north-western Pacific deep-water ventilation (f_{NADW}) is approximately 0.4–0.7. The hydrologically based estimation of the NADW fraction in the far north-western Pacific modern deep-water balance was equal to 0.1–0.3 (Talley, 2011). The remaining part of the deep-water ventilation ($1–f_{NADW}$) in the north-western Pacific belongs to the AABW input, originates around the Antarctic.

The results of the redox-sensitive metals content and $\delta^{18}O_{Ua}$ of core LV 76–21 and other cores recovered over the northern tip of the Emperors have highlighted the variability of the deep-water ventilation and contribution of NADW in the deep water circulation of the far north-western Pacific over the last 43 kyr.

Variability in the total ventilation of the WSG deep water can be approximately estimated from changes in the content of redox-sensitive metals, such as vanadium (Fig. 6B). Variability in the V content of core LV76-21, recovered at the western flank of the Detroit Seamount, showed significant changes in the sediment redox condition, from reduced ones during DO stadials to more oxidized during DOIs (Fig. 6B). This suggests strengthening of the ventilation of the Detroit Seamount deep water during DOIs for MIS 3 and after B/A warming, with some stagnation over the YD.

Meanwhile, records of $\delta^{18}O_{Ua}$ from the LV76-21 core have shown substantial and unusual decreases at intervals of 38.6–36.7 and

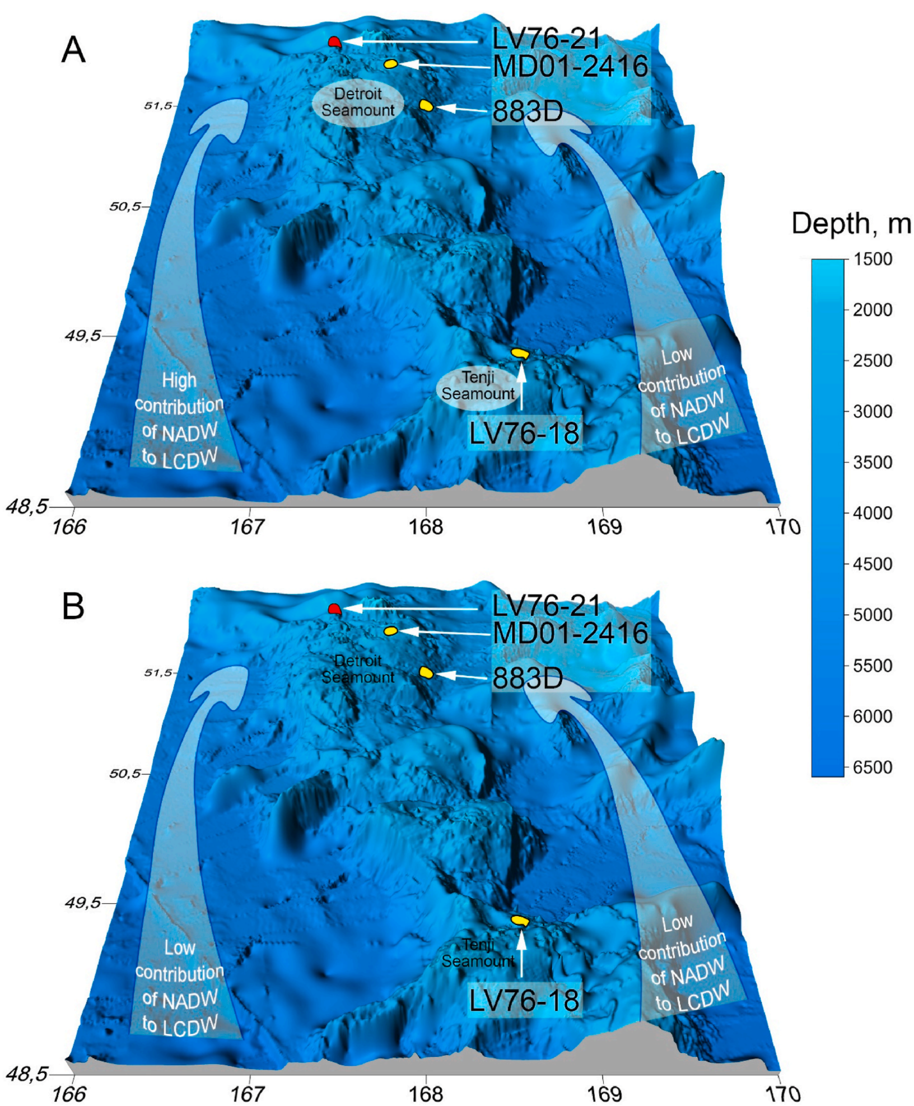

Fig. 7. Schemes of suggested deep-water ventilation for the Detroit–Tenji area during (A) interglacials and long-lasting Dansgaard–Oeschger interstadials (DOI) with a high contribution of NADW to AABW/LCDW on the western slope of the Detroit Seamount, and (B) during glacials and Dansgaard–Oeschger stadials (DOS) with low contribution of NADW to AABW/LCDW on both slopes of the Emperors.

43.6–41.5 ka relative to the coeval $\delta^{18}O_{Ua}$ of other cores MD01-2416 and LV76-18 up to 0.3‰ and 0.5‰, respectively (Fig. 6F; green curve over the green bars). The lightning of $\delta^{18}O_{Ua}$ of the LV76-21 core relative to the coeval $\delta^{18}O_{Ua}$ of other cores cannot be explained by the intensification of the NPIW formation and its penetration to a depth of 2769 m. This is because of the coeval decrease in surface water density, as shown by the lightning of the $\delta^{18}O_{Np}$ values (Fig. 6F, magenta curve). Heavy $\delta^{18}O_{Ua}$ values from several WSG cores during the LGM of approximately 5.2‰ (Fig. 6F) indicate that the NPIW did not reach the bottom of the North Emperor Ridge, including during MIS 2, with maximal deepening of the NPIW in the subarctic Pacific (Keigwin, 1998; Knudson and Ravelo, 2015; Worne et al., 2019). These light deviations in $\delta^{18}O_{Ua}$ record of core LV 76–21 relative to the coeval $\delta^{18}O_{Ua}$ values of other Detroit–Tenji Seamount cores were controlled by changes in the relative contribution of NADW to LCDW in the regional deep-water ventilation. In view of the global ocean deep-water ventilation, Duplessy et al. (2002) concluded that during the LGM the Southern Ocean deep water was extremely cold and close to freezing point. Meanwhile, the Atlantic deep water was approximately 2 °C warmer or, alternatively, there were lighter $\delta^{18}O$ values at temperatures close to freezing. Therefore, observed decreases in the $\delta^{18}O_{Ua}$ record of core LV76-21 relative to ones of other cores during 38.6–36.7 and 43.6–41.5 ka up to 0.3‰ and 0.5‰, respectively, indicated higher contribution of NADW as having lighter $\delta^{18}O$ values to LCDW, which ventilate the deep water at the western slope of the Detroit Seamount (Fig. 7). These lightenings of $\delta^{18}O_{Ua}$ in core LV76-21 corresponded to DOIs 8 and 11, the timespans of intensification of NADW formation, consistently with the conclusions of Böhm et al. (2015). Likely, observed by Böhm et al. (2015) intensification of AMOC and coeval strengthening of NADW formation during DOI for the Atlantic were partly transformed into the North Pacific versus the Antarctic.

During MIS 3, the $\delta^{18}O_{Ua}$ record of core MD01-2416 did not show significant lightenings, including the periods 38.6–36.7 and 43.6–41.5 ka, and tracks parallel with the LR04 stack δ^{18}Obf record. This indicates that during MIS 3, the Eastern Detroit Seamount was bathed predominantly by LCDW with low contribution of NADW (Fig. 7).

During MIS 2 (28–16 ka BP), $\delta^{18}O_{Ua}$ records from cores LV76-21 and MD01-2416, retrieved from the western and eastern slopes of the Detroit Seamount, respectively, demonstrate nearly similar $\delta^{18}O_{Ua}$ values of 5.2–5.1‰ (Fig. 6F). This indicates that these sites were bathed predominantly by LCDW with low contribution of NADW, likely because of the weakening of the AMOC (McManus et al., 2004) Böhm et al. (2015) (Fig. 7B). During the Late Holocene, the $\delta^{18}O_{Ua}$ record of core MD01-2416 reached approximately 4.15–4.2‰ with a total glacial–Late Holocene $\delta^{18}O_{Ua}$ shift of nearly 1‰ (Fig. 6F). Considering the global average $\delta^{18}O$ seawater shift approximately of 1‰ (Schrag et al., 2002) over the LGM–Late Holocene, the $\delta^{18}O_{Ua}$ record of core MD01-2416 indicates small temperature/$\delta^{18}O$ water changes in the local deep water during this time interval. Therefore, from the LGM up to Late Holocene, the eastern slope of the Detroit Seamount was mostly ventilated by the LCDW with very low contribution of NADW, accompanied by small changes in temperature (Fig. 7).

Meanwhile, the $\delta^{18}O_{Ua}$ record for core LV76-21 varies fully in parallel with the δ^{18}Obf stack (Lisiecki and Raymo, 2005) during the Holocene and reached the modern values of approximately 3.4‰ (Fig. 6F). This indicates that, considering the global $\delta^{18}O$ water shift of 1‰, nearly 0.8‰ of $\delta^{18}O_{Ua}$ regional lightning occurred since the LGM because of changes in the temperature and $\delta^{18}O$ of the deep water on the western slope of the Detroit Seamount (Fig. 6F). It is likely that this change in the hydrology of the local deep water was forced by the increase contribution of NADW to LCDW in the deep-water ventilation of the western flank of the Detroit Seamount during the Holocene. The sharp intensification of contribution of NADW to bottom-water ventilation of the western slope of the Detroit Seamount at the onset of B/A warming was also documented in the $\delta^{18}O_{Ua}$ record of core LV76-21 by an abrupt decrease of nearly 0.5‰ (Fig. 6F, green line). This is consistent with the synchronous strengthening of the AMOC formation (McManus et al., 2004) at the onset of B/A warming. This contrasts with the less prominent and steeper changes in the $\delta^{18}O_{Ua}$ record at the eastern slope recorded in core MD01-2416 (Fig. 6F, red curve). During the late Holocene the $\delta^{18}O_{Ua}$ record of core LV76-18 recovered at the northern slope of the Tenji Seamount reach up to 3.8‰, with an average value of $\delta^{18}O_{Ua}$ for cores LV76-21 and MD01-2416 (Fig. 6F). It is likely that the northern slope of Tenji Seamount was ventilated during the Late Holocene by a nearly equal mixture of water with high and low contribution of NADW to LCDW (Fig. 7).

The schemes in Fig. 7 show that the western slope of the Detroit–Tenji Seamounts was ventilated by LCDW with high contribution of NADW during the DOIs of MIS 3 and the interglacials (A) and by the LCDW with low contribution of NADW during the DOSs and glacials (B). Meanwhile, its eastern slope was constantly bathed by LCDW with low contribution of NADW.

5. Conclusions

We constructed an age model for core LV76-21 based on AMS ^{14}C data, δ^{18}Obf records (*Uv. auberiana* and *Cibicidoides* spp.) and tephrochronology, and established correlations between abrupt increases in productivity proxies (calcium carbonate, TOC, chlorin content, BFA, and color b*) and lithological proxies (Rb and Ti content) with DOIs.

A comparison of the LV76-21 core $\delta^{18}O_{Np}$ record with the δ^{18}Obf stack LR04 showed two IDEs in the WSG over the last 43 kyr, namely IDE 1 and IDE 1′, at 39–36.8 and 42–40 ka, respectively. IDE 1 started after DO stadial 9 coeval with an IRD peak and continued during DO cycle 8. IDE 1’ started after DO stadial 11 and continued during DOIs 10–9. We also reconstructed IDEs using similar approaches for the other three dated Detroit and Tenji Seamount cores. However, these ages were approximately 3–2 kyr younger than those obtained for core LV76-21, likely because of inaccuracies in the age models and the strong regional influence of volcanic ash input on WSG sedimentation.

Several proxies responsible for the input of coarse terrigenous and volcanic material in the sediments of the Detroit and Tenji Seamount cores also indicate the high and variable input of the IRD into regional sedimentation during MIS 3 and 2, which were likely primarily delivered by sea ice. During MIS 2, the influence of sea ice on the environment of the study area significantly increased at approximately 28.5–25.5 and 17.6–16.6 ka for SID 2 and 1, respectively. It then dropped to approximately zero after the onset of B/A warming. The formation of SID 2 was likely triggered by a substantial global sea-level drop at approximately 30 ka. This was accompanied by a southward shift of the coastline in the Bering Sea and enhanced sea-ice formation. SID 1 occurred during HE 1, which was the coldest period of the LGM with severe environmental conditions. The influence of sea ice on WSG sedimentation was enhanced during cold YD events.

Dated and highly resolved $\delta^{18}O_{Ua}$ records from the Detroit Seamount cores located on the western and eastern flanks and other Tenji Seamount cores allowed us to evaluate the orbital- and millennial-scale changes in contribution of NADW to LCDW in the deep-water ventilation of the northern tip of the Emperor Seamount Chain over the last 43 kyr. The contribution of the NADW (North Atlantic origin water) to LCDW (Antarctic origin water with its $\delta^{18}O$ values slightly heavier relative to one of the NADW) in the spatial peculiarities of deep-water ventilation of the Detroit–Tenji Seamounts have been estimated based on the coeval variability of the $\delta^{18}O_{Ua}$ of these cores. The $\delta^{18}O_{Ua}$ record of core LV76-21 recovered from the western slope of the Detroit Seamount has provided evidence of the increased contribution of NADW to LCDW in deep-water ventilation of the western flank during the DOIs and Holocene, which was synchronous with AMOC intensification. Based on the $\delta^{18}O_{Ua}$ record of core MD01-2416, the eastern flank of the Detroit Seamount has been constantly ventilated by the LCDW with low contribution of NADW to LCDW over the last 43 kyr. According to the $\delta^{18}O_{Ua}$ record from the Tenji Seamount core, the northern slope was ventilated with mixed

LCDW with high and low contribution of NADW and in nearly equal proportions.

Funding

The cruise during which the core studied was obtained and the primary processing onboard the ship were conducted with financial support from the Marine S&T Fund of Shandong Province for the Pilot National Laboratory for Marine Science and Technology (Qingdao) (number 2022QNML050203), the Taishan Scholar Program of Shandong (tspd20181216), and the Russian state budget (number 121021700342–9 of the POI FEB RAS), part of the work was conducted on the state assignment of the IGM SB RAS. Laboratory and analytical processing of samples and preparation and writing of the manuscript were fully funded by the Russian Science Foundation (number 22-17-00118).

CRediT authorship contribution statement

Sergey A. Gorbarenko: Conceptualization, Writing - original draft. **Xuefa Shi:** Methodology, Investigation. **Aleksandr A. Bosin:** Validation, Investigation. **Yanguang Liu:** Validation, Investigation. **Yuriy P. Vasilenko:** Methodology, Investigation. **Elena A. Yanchenko:** Investigation, Methodology. **Aleksandr N. Derkachev:** Investigation. **Ivan S. Kirichenko:** Investigation, Formal analysis. **Antonina V. Artemova:** Investigation. **Tatyana A. Velivetskaya:** Investigation, oxygen isotopeuu analysis, Galina Yu. Malakhova, Formal analysis, Investigation, Jianjun Zou, Investigation, Validation. **Olga Yu Psheneva:** Validation, Investigation.

Declaration of competing interest

The authors declare that they have no known competing financial interests or personal relationships that could have appeared to influence the work reported in this paper.

Data availability

I have published the file with my data in PANGAEA data repository. Link in the text

Acknowledgments

We would like to thank the two anonymous reviewers and Dr. Ingrid Hendy for their valuable comments, which have substantially improved the paper. We also thank Prof. Pinxian Wang (Tongji University, China) for helping with the $\delta^{18}O$ measurement.

Appendix A. Supplementary data

Supplementary data to this article can be found online at https://doi.org/10.1016/j.quascirev.2023.108472.

References

Alley, R.B., MacAyeal, D.R., 1994. Ice-rafted debris associated with binge/purge oscillations of the Laurentide Ice Sheet. Paleoceanography 9, 503–511. https://doi.org/10.1029/94PA01008.

Altabet, M.A., Higginson, M.J., Murray, D.W., 2002. The effect of millennial-scale changes in Arabian Sea denitrification on atmospheric CO2. Nature 415, 159–162. https://doi.org/10.1038/415159a.

Bigg, G.R., Clark, C.D., Hughes, A.L.C., 2008. A last glacial ice sheet on the Pacific Russian coast and catastrophic change arising from coupled ice–volcanic interaction. Earth Planet Sci. Lett. 265, 559–570. https://doi.org/10.1016/j.epsl.2007.10.052.

Bindeman, I.N., Leonov, V.L., Izbekov, P.E., Ponomareva, V.V., Watts, K.E., Shipley, N.K., Perepelov, A.B., Bazanova, L.I., Jicha, B.R., Singer, B.S., Schmitt, A.K., Portnyagin, M.V., Chen, C.H., 2010. Large-volume silicic volcanism in Kamchatka: Ar–Ar and U–Pb ages, isotopic, and geochemical characteristics of major pre-Holocene caldera-forming eruptions. J. Volcanol. Geoth. Res. 189, 57–80. https://doi.org/10.1016/j.jvolgeores.2009.10.009.

Blaauw, M., Christen, J.A., 2011. Flexible paleoclimate age-depth models using an autoregressive gamma process. Bayesian Anal 6. https://doi.org/10.1214/11-BA618.

Bodin, S., Godet, A., Matera, V., Steinmann, P., Vermeulen, J., Gardin, S., Adatte, T., Coccioni, R., Föllmi, K.B., 2007. Enrichment of redox-sensitive trace metals (U, V, Mo, As) associated with the late Hauterivian Faraoni oceanic anoxic event. Int. J. Earth Sci. 96, 327–341. https://doi.org/10.1007/s00531-006-0091-9.

Böhm, E., Lippold, J., Gutjahr, M., Frank, M., Blaser, P., Antz, B., Fohlmeister, J., Frank, N., Andersen, M.B., Deininger, M., 2015. Strong and deep Atlantic meridional overturning circulation during the last glacial cycle. Nature 517, 73–76. https://doi.org/10.1038/nature14059.

Bond, G., Broecker, W., Johnsen, S., McManus, J., Labeyrie, L., Jouzel, J., Bonani, G., 1993. Correlations between climate records from North Atlantic sediments and Greenland ice. Nature 365, 143–147. https://doi.org/10.1038/365143a0.

Braitseva, O.A., Melekestsev, I.V., Sulerzhitskii, L.D., 2005. New data on the Pleistocene deposits age in the Central Kamchatka depression. Stratigr. Geol. Correl. 13, 99–107.

Braitseva, O.A., Melekestsev, I.V., Ponomareva, V.V., Sulerzhitsky, L.D., 1995. Ages of calderas, large explosive craters and active volcanoes in the Kuril-Kamchatka region, Russia. Bull. Volcanol. 57, 383–402. https://doi.org/10.1007/BF00300984.

Brigham-Grette, J., Gualtieri, L.M., Glushkova, O.Y., Hamilton, T.D., Mostoller, D., Kotov, A., 2003. Chlorine-36 and 14 C chronology support a limited last glacial maximum across central Chukotka, northeastern Siberia, and no Beringian ice sheet. Quat. Res. 59, 386–398. https://doi.org/10.1016/S0033-5894(03)00058-9.

Broecker, W., 1991. The great ocean conveyor. Oceanography 4, 79–89. https://doi.org/10.5670/oceanog.1991.07.

Butzin, M., Köhler, P., Lohmann, G., 2017. Marine radiocarbon reservoir age simulations for the past 50,000 years. Geophys. Res. Lett. 44, 8473–8480. https://doi.org/10.1002/2017GL074688.

Cheng, H., Edwards, R.L., Wang, Y., Kong, X., Ming, Y., Kelly, M.J., Wang, X., Gallup, C.D., Liu, W., 2006. A penultimate glacial monsoon record from Hulu Cave and two-phase glacial terminations. Geology 34, 217. https://doi.org/10.1130/G22289.1.

Colman, S.M., Peck, J.A., Karabanov, E.B., Carter, S.J., Bradbury, J.P., King, J.W., Williams, D.F., 1995. Continental climate response to orbital forcing from biogenic silica records in Lake Baikal. Nature 378, 769–771. https://doi.org/10.1038/378769a0.

Conolly, J.R., Ewing, M., 1970. Ice-rafted detritus in northwest Pacific deep-sea sediments. In: Hays, J.D. (Ed.), Geological Investigations of the North Pacific. Geological Society of America, Boulder, Colorado, pp. 219–231.

Corrick, E.C., Drysdale, R.N., Hellstrom, J.C., Capron, E., Rasmussen, S.O., Zhang, X., Fleitmann, D., Couchoud, I., Wolff, E., 2020. Synchronous timing of abrupt climate changes during the last glacial period. Science 369, 963–969. https://doi.org/10.1126/science.aay5538, 80-.

Dansgaard, W., Clausen, H.B., Gundestrup, N., Hammer, C.U., Johnsen, S.F., Kristinsdottir, P.M., Reeh, N., 1982. A new Greenland deep ice core. Science 218, 1273–1277. https://doi.org/10.1126/science.218.4579.1273, 80-.

Dansgaard, W., Johnsen, S.J., Clausen, H.B., Dahl-Jensen, D., Gundestrup, N.S., Hammer, C.U., Hvidberg, C.S., Steffensen, J.P., Sveinbjörnsdóttir, A.E., Jouzel, J., Bond, G.C., 1993. Evidence for general instability of past climate from a 250-kyr ice-core record. Nature 364, 218–220. https://doi.org/10.1038/364218a0.

Derkachev, A., Gorbarenko, S., Portnyagin, M., Zhong, Y., Nikolaeva, N., Shi, X., Liu, Y., 2023. Tephrostratigraphy of Pleistocene-Holocene deposits from the Detroit Rise eastern slope (northwestern Pacific). Front. Earth Sci. 10 https://doi.org/10.3389/feart.2022.971404.

Duplessy, J.-C., Labeyrie, L.D., Waelbroeck, C., 2002. Constraints on the ocean oxygen isotopic enrichment between the last glacial maximum and the Holocene: paleoceanographic implications. Quat. Sci. Rev. 21, 315–330. https://doi.org/10.1016/S0277-3791(01)00107-X.

Emile-Geay, J., Cane, M.A., Naik, N., Seager, R., Clement, A.C., van Geen, A., 2003. Warren revisited: atmospheric freshwater fluxes and "Why is no deep water formed in the North Pacific.". J. Geophys. Res. 108, 3178. https://doi.org/10.1029/2001JC001058.

Favorite, F., Dodimead, A.J.J., Nasu, K., 1976. Oceanography of the subarctic Pacific region. In: International North Pacific Fisheries Commission, p. 187, 1960-71.

Fuhr, M., Laukert, G., Yu, Y., Nürnberg, D., Frank, M., 2021. Tracing water mass mixing from the equatorial to the North Pacific ocean with dissolved neodymium isotopes and concentrations. Front. Mar. Sci. 7 https://doi.org/10.3389/fmars.2020.603761.

Galbraith, E.D., Jaccard, S.L., Pedersen, T.F., Sigman, D.M., Haug, G.H., Cook, M.S., Southon, J.R., Francois, R., 2007. Carbon dioxide release from the North Pacific abyss during the last deglaciation. Nature 449, 890–893. https://doi.org/10.1038/nature06227.

Gebhardt, H., Sarnthein, M., Grootes, P.M., Kiefer, T., Kuehn, H., Schmieder, F., Röhl, U., 2008. Paleonutrient and productivity records from the subarctic North Pacific for Pleistocene glacial terminations I to V. Paleoceanography 23. https://doi.org/10.1029/2007PA001513.

Gebregiorgis, D., Hathorne, E.C., Sijinkumar, A.V., Nath, B.N., Nürnberg, D., Frank, M., 2016. South Asian summer monsoon variability during the last ~54 kyrs inferred from surface water salinity and river runoff proxies. Quat. Sci. Rev. 138, 6–15. https://doi.org/10.1016/j.quascirev.2016.02.012.

Goldberg, E.L., Phedorin, M.A., Chebykin, E.P., Zolotarev, K.V., Zhuchenko, N.A., 2007. Decade–centenary resolution records of climate changes in East Siberia from elements in the bottom sediments of lake Baikal for the last 150kyr. Nucl. Instruments Methods Phys. Res. Sect. A Accel. Spectrometers, Detect. Assoc. Equip. 575, 193–195. https://doi.org/10.1016/j.nima.2007.01.065.

Gorbarenko, S.A., Chebykin, E.P., Goldberg, E.L., Stepanova, O.G., Lu, H., 2014. Chronicle of regional volcanic eruptions recorded in Okhotsk Sea sediments over the last 350 ka. Quat. Geochronol. 20, 29–38. https://doi.org/10.1016/j.quageo.2013.10.006.

Gorbarenko, S.A., Chekhovskaya, M.P., Southon, J.R., 1998. On the paleoenvironment of the central part of the Sea of Okhotsk during the past Holocene glaciation. Oceanology 38, 277–280.

Gorbarenko, S.A., Harada, N., Malakhov, M.I., Vasilenko, Y.P., Bosin, A.A., Goldberg, E.L., 2010. Orbital and millennial-scale environmental and sedimentological changes in the Okhotsk Sea during the last 350kyr. Global Planet. Change 72, 79–85. https://doi.org/10.1016/j.gloplacha.2010.03.002.

Gorbarenko, S.A., Shi, X., Liu, Y., Vasilenko, Y.P., Yanchenko, E.A., Derkachev, A.N., Bosin, A.A., Velivetskaya, T.A., Malakhova, G.Y., Zou, J., Kirichenko, I.S., Artemova, A.V., Psheneva, O.Y., 2022. Iceberg discharge events in the northwest Pacific and related sequence of Kamchatka glaciations over the last 190 kyr. Quat. Sci. Rev. 278, 107349 https://doi.org/10.1016/j.quascirev.2021.107349.

Grootes, P.M., Stuiver, M., White, J.W.C., Johnsen, S., Jouzel, J., 1993. Comparison of oxygen isotope records from the GISP2 and GRIP Greenland ice cores. Nature 366, 552–554. https://doi.org/10.1038/366552a0.

Grosswald, M.G., Hughes, T.J., 2002. The Russian component of an arctic ice sheet during the last glacial maximum. Quat. Sci. Rev. 21, 121–146. https://doi.org/10.1016/S0277-3791(01)00078-6.

Gupta, A.K., Sarkar, S., Mukherjee, B., 2006. Paleoceanographic changes during the past 1.9 Myr at DSDP site 238, central Indian ocean basin: benthic foraminiferal proxies. Mar. Micropaleontol. 60, 157–166. https://doi.org/10.1016/j.marmicro.2006.04.001.

Harris, P.G., Zhao, M., Rosell-Melé, A., Tiedemann, R., Sarnthein, M., Maxwell, J.R., 1996. Chlorin accumulation rate as a proxy for Quaternary marine primary productivity. Nature 383, 63–65. https://doi.org/10.1038/383063a0.

Heinrich, H., 1988. Origin and consequences of cyclic ice rafting in the Northeast Atlantic Ocean during the past 130,000 years. Quat. Res. 29, 142–152. https://doi.org/10.1016/0033-5894(88)90057-9.

Hemming, S.R., 2004. Heinrich events: massive late Pleistocene detritus layers of the North Atlantic and their global climate imprint. Rev. Geophys. 42, RG1005. https://doi.org/10.1029/2003RG000128.

Hendy, I., Kennett, J., Roark, E., Ingram, B., 2002. Apparent synchroneity of submillennial scale climate events between Greenland and Santa Barbara Basin, California from 30–10ka. Quat. Sci. Rev. 21, 1167–1184. https://doi.org/10.1016/S0277-3791(01)00138-X.

Hendy, I.L., Kennett, J.P., 1999. Latest Quaternary North Pacific surface-water responses imply atmosphere-driven climate instability. Geology 27, 291. https://doi.org/10.1130/0091-7613(1999)027<0291:LQNPSW>2.3.CO, 2.

Jaccard, S.L., Galbraith, E.D., Sigman, D.M., Haug, G.H., 2010. A pervasive link between Antarctic ice core and subarctic Pacific sediment records over the past 800 kyrs. Quat. Sci. Rev. 29, 206–212. https://doi.org/10.1016/j.quascirev.2009.10.007.

Jaccard, S.L., Haug, G.H., Sigman, D.M., Pedersen, T.F., Thierstein, H.R., Röhl, U., 2005. Glacial/interglacial changes in subarctic north pacific stratification. Science 308, 1003–1006. https://doi.org/10.1126/science.1108696.

Johnsen, S.J., Clausen, H.B., Dansgaard, W., Fuhrer, K., Gundestrup, N.S., Hammer, C.U., Iversen, P., Jouzel, J., Stauffer, B., Steffensen, J.P., 1992. Irregular glacial interstadials recorded in a new Greenland ice core. Nature 359, 311–313. https://doi.org/10.1038/359311a0.

Johnson, G.C., 2008. Quantifying antarctic bottom water and North Atlantic deep water volumes. J. Geophys. Res. 113, C05027 https://doi.org/10.1029/2007JC004477.

Jones, R.T., Marshall, J.D., Crowley, S.F., Bedford, A., Richardson, N., Bloemendal, J., Oldfield, F., 2002. A high resolution, multiproxy Late-glacial record of climate change and intrasystem responses in northwest England. J. Quat. Sci. 17, 329–340. https://doi.org/10.1002/jqs.683.

Jorissen, F.J., Fontanier, C., Thomas, E., 2007. Chapter seven paleoceanographical proxies based on deep-sea benthic foraminiferal assemblage characteristics. In: Developments in Marine Geology, pp. 263–325. https://doi.org/10.1016/S1572-5480(07)01012-3.

Kawabe, M., Fujio, S., 2010. Pacific ocean circulation based on observation. J. Oceanogr. 66, 389–403. https://doi.org/10.1007/s10872-010-0034-8.

Keigwin, L.D., 1998. Glacial-age hydrography of the far northwest Pacific Ocean. Paleoceanography 13, 323–339. https://doi.org/10.1029/98PA00874.

Keigwin, L.D., Jones, G.A., Froelich, P.N., 1992. A 15,000 year paleoenvironmental record from Meiji Seamount, far northwestern Pacific. Earth Planet Sci. Lett. 111, 425–440. https://doi.org/10.1016/0012-821X(92)90194-Z.

Kiefer, T., Sarnthein, M., Erlenkeuser, H., Grootes, P.M., Roberts, A.P., 2001. North Pacific response to millennial-scale changes in ocean circulation over the last 60 kyr. Paleoceanography 16, 179–189. https://doi.org/10.1029/2000PA000545.

Kienast, S.S., McKay, J.L., 2001. Sea surface temperature in the subartic Northeast Pacific reflect millennial-scale climate oscillations during the last 16 kyr. Geophys. Res. Lett. 28, 1563–1566.

Knudson, K.P., Ravelo, A.C., 2015. North pacific intermediate water circulation enhanced by the closure of the bering strait. Paleoceanography 30, 1287–1304. https://doi.org/10.1002/2015PA002840.

Lambeck, K., Rouby, H., Purcell, A., Sun, Y., Sambridge, M., 2014. Sea level and global ice volumes from the last glacial maximum to the Holocene. Proc. Natl. Acad. Sci. USA 111, 15296–15303. https://doi.org/10.1073/pnas.1411762111.

Lisiecki, L.E., Raymo, M.E., 2005. A Pliocene-Pleistocene stack of 57 globally distributed benthic δ 18 O records. Paleoceanography 20, PA1003. https://doi.org/10.1029/2004PA001071.

Lisitzin, A.P., 2002. Sea-Ice and Iceberg Sedimentation in the Ocean. Springer, Berlin, Heidelberg. https://doi.org/10.1007/978-3-642-55905-1.

Mackensen, A., Schumacher, S., Radke, J., Schmidt, D.N., 2000. Microhabitat preferences and stable carbon isotopes of endobenthic foraminifera: clue to quantitative reconstruction of oceanic new production? Mar. Micropaleontol. 40, 233–258. https://doi.org/10.1016/S0377-8398(00)00040-2.

Maier, E., Zhang, X., Abelmann, A., Gersonde, R., Mulitza, S., Werner, M., Méheust, M., Ren, J., Chapligin, B., Meyer, H., Stein, R., Tiedemann, R., Lohmann, G., 2018. North Pacific freshwater events linked to changes in glacial ocean circulation. Nature 559, 241–245. https://doi.org/10.1038/s41586-018-0276-y.

Markle, B.R., Steig, E.J., Buizert, C., Schoenemann, S.W., Bitz, C.M., Fudge, T.J., Pedro, J.B., Ding, Q., Jones, T.R., White, J.W.C., Sowers, T., 2017. Global atmospheric teleconnections during Dansgaard–Oeschger events. Nat. Geosci. 10, 36–40. https://doi.org/10.1038/ngeo2848.

Matsumoto, K., 2007. Radiocarbon-based circulation age of the world oceans. J. Geophys. Res. 112, C09004 https://doi.org/10.1029/2007JC004095.

Max, L., Riethdorf, J.-R., Tiedemann, R., Smirnova, M.A., Lembke-Jene, L., Fahl, K., Nürnberg, D., Matul, A.G., Mollenhauer, G., 2012. Sea surface temperature variability and sea-ice extent in the subarctic northwest Pacific during the past 15,000 years. Paleoceanography 27. https://doi.org/10.1029/2012PA002292.

Mayewski, P.A., Meeker, L.D., Twickler, M.S., Whitlow, S., Yang, Q., Lyons, W.B., Prentice, M., 1997. Major features and forcing of high-latitude northern hemisphere atmospheric circulation using a 110,000-year-long glaciochemical series. J. Geophys. Res. Ocean. 102, 26345–26366. https://doi.org/10.1029/96JC03365.

McCarron, A.P., Bigg, G.R., Brooks, H., Leng, M.J., Marshall, J.D., Ponomareva, V., Portnyagin, M., Reimer, P.J., Rogerson, M., 2021. Northwest Pacific ice-rafted debris at 38°N reveals episodic ice-sheet change in late Quaternary Northeast Siberia. Earth Planet Sci. Lett. 553, 116650 https://doi.org/10.1016/j.epsl.2020.116650.

McKelvey, B.C., Chen, W., Arculus, R.J., 1995. Provenance of pliocene-pleistocene ice-rafted debris, leg 145, northern pacific ocean. In: Rea, D.K., Basov, I.A., Scholl, D.W., Allan, J.F. (Eds.), Proceedings of the Ocean Drilling Program, 145 Scientific Results. Ocean Drilling Program, pp. 195–204. https://doi.org/10.2973/odp.proc.sr.145.120.1995.

McManus, J.F., Francois, R., Gherardi, J.-M., Keigwin, L.D., Brown-Leger, S., 2004. Collapse and rapid resumption of Atlantic meridional circulation linked to deglacial climate changes. Nature 428, 834–837. https://doi.org/10.1038/nature02494.

NGRIP members, 2004. High-resolution record of Northern Hemisphere climate extending into the last interglacial period. Nature 431, 147–151. https://doi.org/10.1038/nature02805.

Nürnberg, D., Tiedemann, R., 2004. Environmental change in the Sea of Okhotsk during the last 1.1 million years. Paleoceanography 19. https://doi.org/10.1029/2004PA001023 n/a-n/a.

Ohkushi, K., Thomas, E., Kawahata, H., 2000. Abyssal benthic foraminifera from the northwestern Pacific (Shatsky Rise) during the last 298 kyr. Mar. Micropaleontol. 38, 119–147. https://doi.org/10.1016/S0377-8398(99)00040-7.

Owens, W.B., Warren, B.A., 2001. Deep circulation in the northwest corner of the Pacific Ocean. Deep-Sea Res. Part I Oceanogr. Res. Pap. 48, 959–993. https://doi.org/10.1016/S0967-0637(00)00076-5.

Phedorin, M.A., Fedotov, A.P., Saeva, O.P., Bobrov, V.A., 2007. Variations in environmental conditions of intracontinental Asia over the past 1 Ma in high-resolution geochemical records from bottom sediments of Lake Khubsugul (Mongolia). Dokl. Earth Sci. 417, 1416–1420. https://doi.org/10.1134/S1028334X07090267.

Piminov, P.A., Baranov, G.N., Bogomyagkov, A.V., Berkaev, D.E., Borin, V.M., Dorokhov, V.L., Karnaev, S.E., Kiselev, V.A., Levichev, E.B., Meshkov, O.I., Mishnev, S.I., Nikitin, S.A., Nikolaev, I.B., Sinyatkin, S.V., Vobly, P.D., Zolotarev, K.V., Zhuravlev, A.N., 2016. Synchrotron radiation research and application at VEPP-4. Phys. Procedia 84, 19–26. https://doi.org/10.1016/j.phpro.2016.11.005.

Ponomareva, V., Pendea, I.F., Zelenin, E., Portnyagin, M., Gorbach, N., Pevzner, M., Plechova, A., Derkachev, A., Rogozin, A., Garbe-Schönberg, D., 2021. The first continuous late Pleistocene tephra record from Kamchatka Peninsula (NW Pacific) and its volcanological and paleogeographic implications. Quat. Sci. Rev. 257, 106838 https://doi.org/10.1016/j.quascirev.2021.106838.

Ponomareva, V.V., Portnyagin, M.V., Derkachev, A.N., Bazanova, L.I., Bubenshchikova, N.V., Zelenin, E.A., Rogozin, A., Plechova, A., Gorbarenko, S.A., 2017. A 7.2 Ma tephra sequence at the Detroit Seamount, NW Pacific: a key reference for regional correlatons and record of major explosive eruptions from North Pacific volcanic arcs. In: XXII МеЖдународная Научная Конференция (Школа) По Морской Геологии "Геология Морей и Океанов". Москва, 20–24 Ноября 2017 Года, pp. 277–281.

Rahmstorf, S., 2002. Ocean circulation and climate during the past 120,000 years. Nature 419, 207–214. https://doi.org/10.1038/nature01090.

Rasmussen, S.O., Bigler, M., Blockley, S.P., Blunier, T., Buchardt, S.L., Clausen, H.B., Cvijanovic, I., Dahl-Jensen, D., Johnsen, S.J., Fischer, H., Gkinis, V., Guillevic, M., Hoek, W.Z., Lowe, J.J., Pedro, J.B., Popp, T.J., Seierstad, I.K., Steffensen, J.P., Svensson, A.M., Vallelonga, P., Vinther, B.M., Walker, M.J.C., Wheatley, J.J., Winstrup, M., 2014. A stratigraphic framework for abrupt climatic changes during the Last Glacial period based on three synchronized Greenland ice-core records: refining and extending the INTIMATE event stratigraphy. Quat. Sci. Rev. 106, 14–28. https://doi.org/10.1016/j.quascirev.2014.09.007.

Reimer, P.J., Austin, W.E.N., Bard, E., Bayliss, A., Blackwell, P.G., Bronk Ramsey, C., Butzin, M., Cheng, H., Edwards, R.L., Friedrich, M., Grootes, P.M., Guilderson, T.P., Hajdas, I., Heaton, T.J., Hogg, A.G., Hughen, K.A., Kromer, B., Manning, S.W., Muscheler, R., Palmer, J.G., Pearson, C., van der Plicht, J., Reimer, R.W., Richards, D.A., Scott, E.M., Southon, J.R., Turney, C.S.M., Wacker, L., Adolphi, F., Büntgen, U., Capano, M., Fahrni, S.M., Fogtmann-Schulz, A., Friedrich, R., Köhler, P., Kudsk, S., Miyake, F., Olsen, J., Reinig, F., Sakamoto, M., Sookdeo, A., Talamo, S., 2020. The IntCal20 northern hemisphere radiocarbon age calibration

curve (0–55 cal kBP). Radiocarbon 62, 725–757. https://doi.org/10.1017/RDC.2020.41.
Riethdorf, J.-R., Nürnberg, D., Max, L., Tiedemann, R., Gorbarenko, S.A., Malakhov, M.I., 2013. Millennial-scale variability of marine productivity and terrigenous matter supply in the western Bering Sea over the past 180 kyr. Clim. Past 9, 1345–1373. https://doi.org/10.5194/cp-9-1345-2013.
Sarnthein, M., Grootes, P.M., Kennett, J.P., Nadeau, M.-J., 2007. 14C reservoir ages show deglacial changes in ocean currents and carbon cycle. In: Ocean Circulation: Mechanisms and Impacts—Past and Future Changes of Meridional Overturning, pp. 175–196. https://doi.org/10.1029/173GM13.
Schlung, S.A., Ravelo, C.A., Aiello, I.W., Andreasen, D.H., Cook, M.S., Drake, M., Dyez, K. A., Guilderson, T.P., LaRiviere, J.P., Stroynowski, Z., Takahashi, K., 2013. Millennial-scale climate change and intermediate water circulation in the Bering Sea from 90 ka: a high-resolution record from IODP Site U1340. Paleoceanography 28, 54–67. https://doi.org/10.1029/2012PA002365.
Schrag, D.P., Adkins, J.F., McIntyre, K., Alexander, J.L., Hodell, D.A., Charles, C.D., McManus, J.F., 2002. The oxygen isotopic composition of seawater during the Last Glacial Maximum. Quat. Sci. Rev. 21, 331–342. https://doi.org/10.1016/S0277-3791(01)00110-X.
Schulz, H., von Rad, U., Erlenkeuser, H., von Rad, U., 1998. Correlation between Arabian Sea and Greenland climate oscillations of the past 110,000 years. Nature 393, 54–57. https://doi.org/10.1038/31750.
Seki, O., Ishiwatari, R., Matsumoto, K., 2002. Millennial climate oscillations in NE Pacific surface waters over the last 82 kyr: new evidence from alkenones. Geophys. Res. Lett. 29, 59. https://doi.org/10.1029/2002GL015200, 1-59–4.
Shackleton, N.J., 1974. Attainment of isotopic equilibrium between ocean water and the benthonic foraminifera genus Uvigerina: isotopic changes in the ocean during the last glacial. In: Les Methodes Quantitatives D'Etude Des Variations Du Climat Au Cours Du Pleistocene. Gif sur Yvette, pp. 203–209.
Shakun, J.D., Clark, P.U., He, F., Marcott, S.A., Mix, A.C., Liu, Z., Otto-Bliesner, B., Schmittner, A., Bard, E., 2012. Global warming preceded by increasing carbon dioxide concentrations during the last deglaciation. Nature 484, 49–54. https://doi.org/10.1038/nature10915.
Stuiver, M., Quay, P.D., Ostlund, H.G., 1983. Abyssal water carbon-14 distribution and the age of the world oceans. Science 84 219, 849–851. https://doi.org/10.1126/science.219.4586.849.
Talley, L., 2013. Closure of the global overturning circulation through the Indian, pacific, and southern oceans: schematics and transports. Oceanography 26, 80–97. https://doi.org/10.5670/oceanog.2013.07.
Talley, L.D., 2011. Descriptive Physical Oceanography: an Introduction. Academic Press.
Talley, L.D., 1993. Distribution and formation of North Pacific intermediate water. J. Phys. Oceanogr. 23, 517–537. https://doi.org/10.1175/1520-0485(1993)023<0517:DAFONP>2.0.CO, 2.
VanLaningham, S., Pisias, N.G., Duncan, R.A., Clift, P.D., 2009. Glacial–interglacial sediment transport to the meiji drift, northwest Pacific ocean: evidence for timing of beringian outwashing. Earth Planet Sci. Lett. 277, 64–72. https://doi.org/10.1016/j.epsl.2008.09.033.
Velivetskaya, T.A., Ignatiev, A.V., Gorbarenko, S.A., 2009. Carbon and oxygen isotope microanalysis of carbonate. Rapid Commun. Mass Spectrom. 23, 2391–2397. https://doi.org/10.1002/rcm.3989.
Wang, Y., Cheng, H., Edwards, R.L., An, Z., Wu, J., Shen, C.-C., Dorale, J.A., 2001. A high-resolution absolute-dated late Pleistocene Monsoon record from Hulu Cave, China. Science 294, 2345–2348. https://doi.org/10.1126/science.1064618.
Warren, B.A., 1983. Why is no deep water formed in the North Pacific? J. Mar. Res. 41, 327–347. https://doi.org/10.1357/002224083788520207.
Worne, S., Kender, S., Swann, G.E.A., Leng, M.J., Ravelo, A.C., 2019. Coupled climate and subarctic Pacific nutrient upwelling over the last 850,000 years. Earth Planet Sci. Lett. 522, 87–97. https://doi.org/10.1016/j.epsl.2019.06.028.
Yokoyama, Y., Esat, T.M., Thompson, W.G., Thomas, A.L., Webster, J.M., Miyairi, Y., Sawada, C., Aze, T., Matsuzaki, H., Okuno, J., Fallon, S., Braga, J.-C., Humblet, M., Iryu, Y., Potts, D.C., Fujita, K., Suzuki, A., Kan, H., 2018. Rapid glaciation and a two-step sea level plunge into the Last Glacial Maximum. Nature 559, 603–607. https://doi.org/10.1038/s41586-018-0335-4.
Zakharkov, S.P., Gorbarenko, S.A., Bosin, A.A., 2007. Chlorin content in sea sediments as an indication of sea primary productivity. Bull. Far East. Branch Russ. Acad. Sci. 1, 52–58 (in Russian).